Supporting Information

Understanding the varying mechanisms between the conformal interlayer and overlayer in the silicon/hematite dual-absorber photoanode for solar water splitting

Zhongyuan Zhou,[a,b] Liujing Li,[b] Yongsheng Niu,[a] Haixiang Song,[a] Xiu-Shuang Xing,[*c] Zhanhu Guo,[d] and Shaolong Wu[*b,e]

[a]Henan Joint International Research Laboratory of Nanocomposite Sensing Materials, School of Chemical and Environmental Engineering, Anyang Institute of Technology, Anyang 455000, China.

[b]School of Optoelectronic Science and Engineering, Soochow University, Suzhou 215006, China.

[c]School of Chemistry and Chemical Engineering, Anyang Normal University, Anyang 455000, China.

[d]Integrated Composites Laboratory (ICL), Department of Chemical & Biomolecular Engineering, University of Tennessee, Knoxville, Tennessee 37996, USA.

[e]Light Industry Institute of Electrochemical Power Sources, Suzhou 215006, China.

[*]Email: xsxing0621@163.com; shaolong_wu@suda.edu.cn

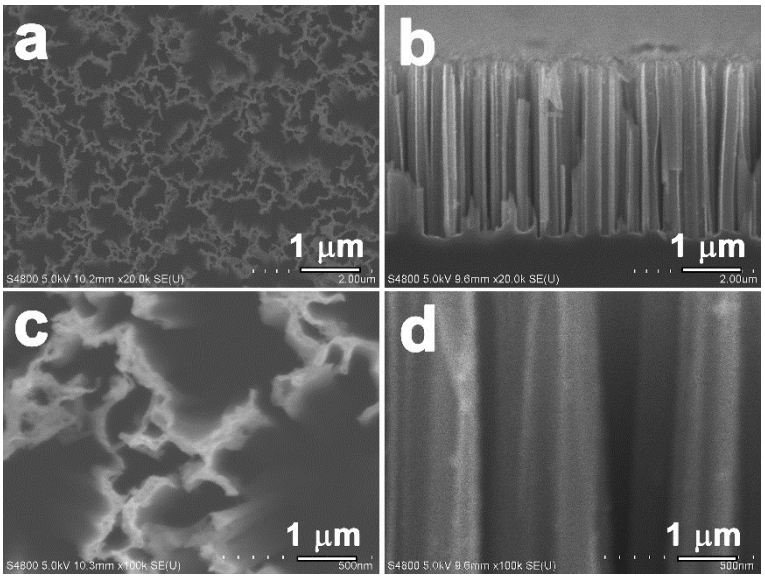

Fig. S1 SEM images of the as-prepared SiNWs. (a and b) are the top-view and cross-section SEM images, (c and d) are the detailed views of the top and side regions, respectively.

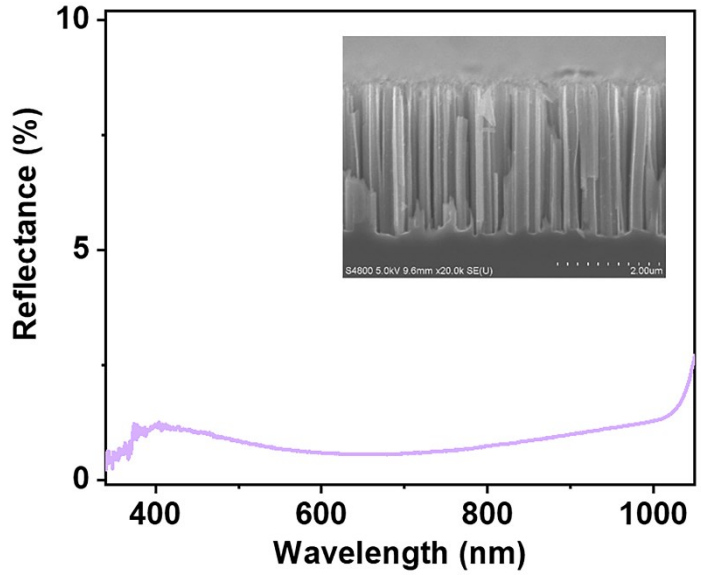

Fig. S2 Reflectance spectrum of the as-prepared SiNWs with the length of ~3 μm, and the insert is the corresponding SEM image.

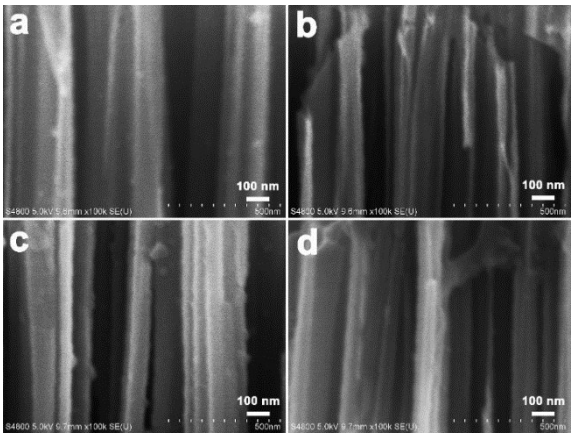

Fig. S3 Detailed SEM images of the side regions in the prepared (a) SiNWs, (b) SiNWs/Sn@α-Fe_2O_3, (c) SiNWs/Sn@α-Fe_2O_3/Al_2O_3 and (d) SiNWs/Al_2O_3/Sn@α-Fe_2O_3.

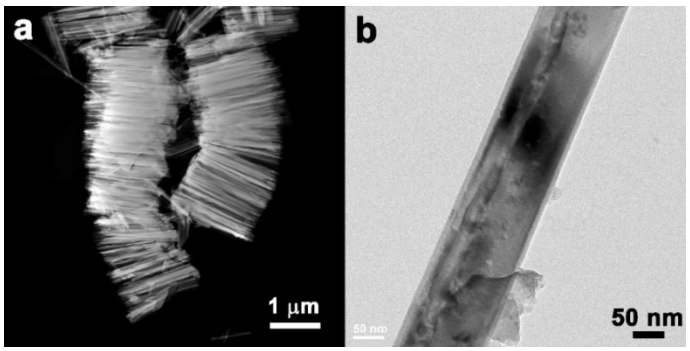

Fig. S4 TEM images of the Si/Sn@α-Fe_2O_3 nanowire heterostructures scraped from the substrate.

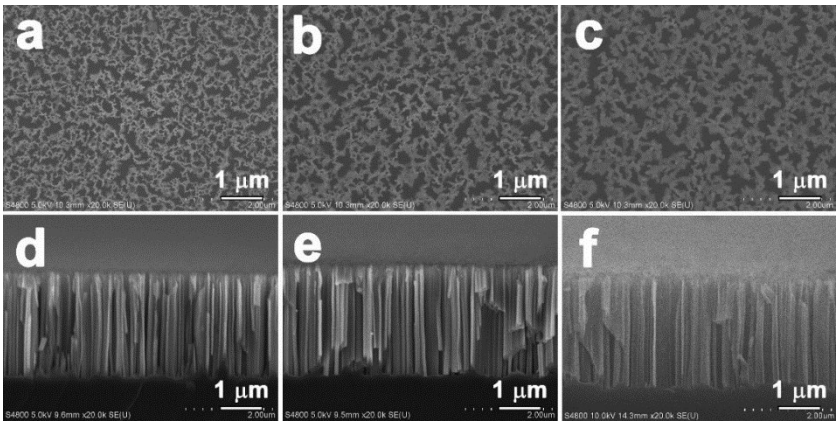

Fig. S5 SEM images of the SiNWs/Al_2O_3 photoanodes with different thicknesses of Al_2O_3 film. (a–c) and (d–f) are the top-view and cross-section SEM images, respectively. (a and d), (b and e) and (c and f) represent the 10, 50 and 100 ALD-cycle Al_2O_3 coated on the SiNWs, respectively.

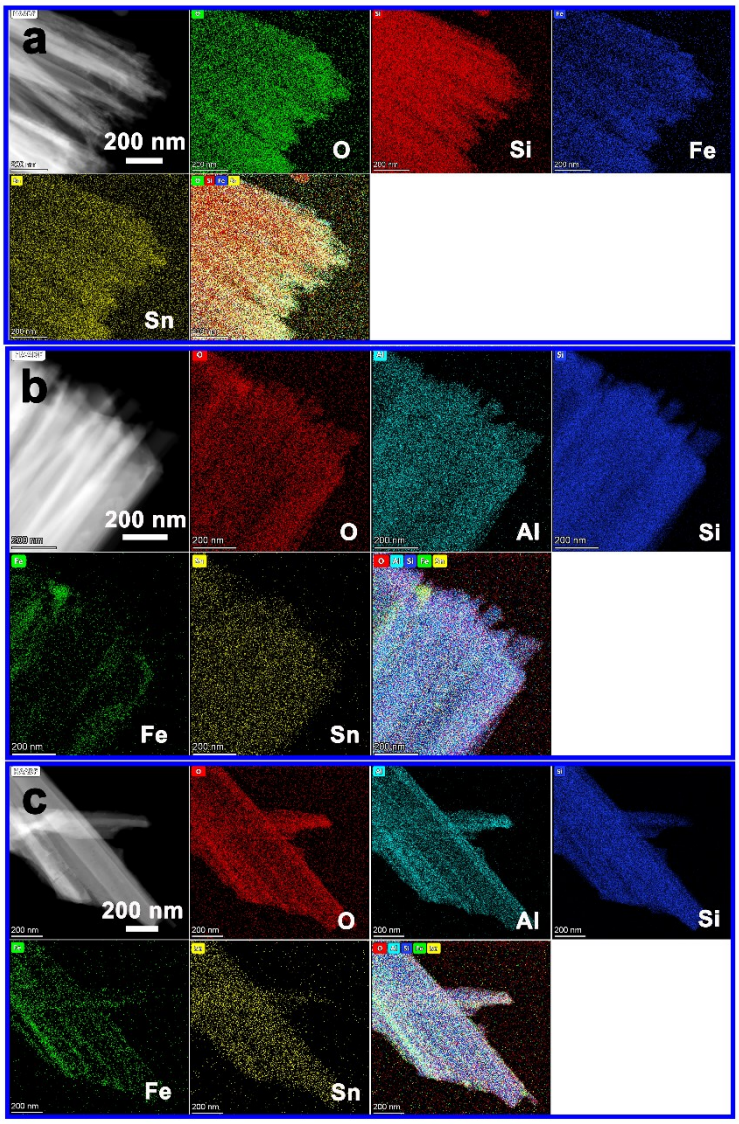

Fig. S6 STEM-HAADF analysis of the (a) SiNWs/Sn@α-Fe_2O_3, (b) SiNWs/Sn@α-Fe_2O_3/Al_2O_3 and (c) SiNWs/Al_2O_3/Sn@α-Fe_2O_3 nanowire heterostructures, respectively.

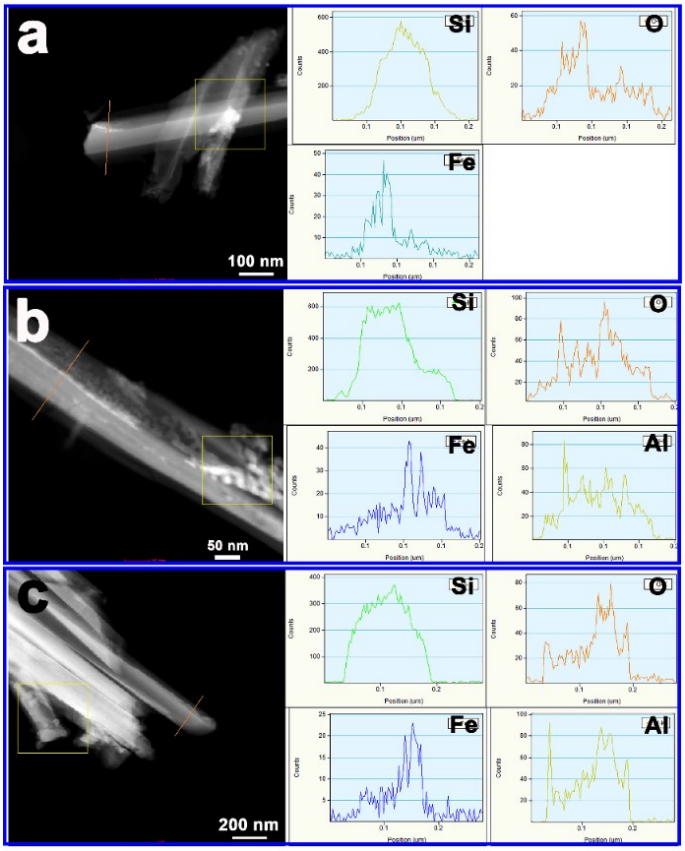

Fig. S7. STEM-EDS comparison in the (a) SiNWs/Sn@α-Fe_2O_3, (b) SiNWs/Sn@α-Fe_2O_3/Al_2O_3 and (c) SiNWs/Al_2O_3/Sn@α-Fe_2O_3 nanowire heterostructures, respectively.

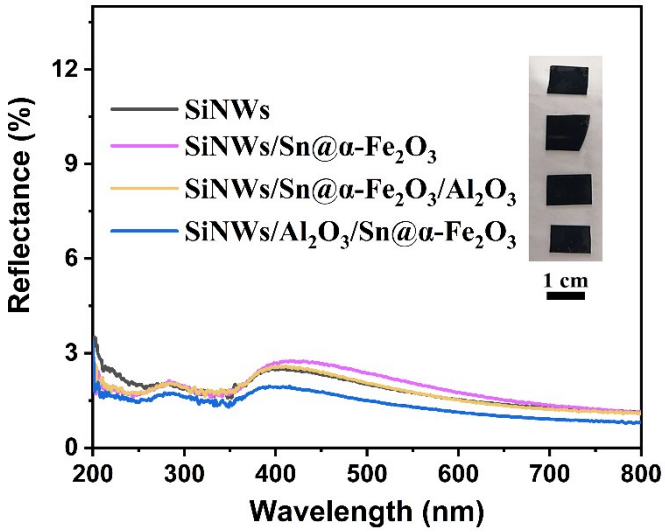

Fig. S8 Reflectance spectra of the as-prepared SiNWs, SiNWs/Sn@α-Fe_2O_3, SiNWs/Sn@α-Fe_2O_3/Al_2O_3 and SiNWs/Al_2O_3/Sn@α-Fe_2O_3 photoanodes. The corresponding digital photographs are shown in the insert.

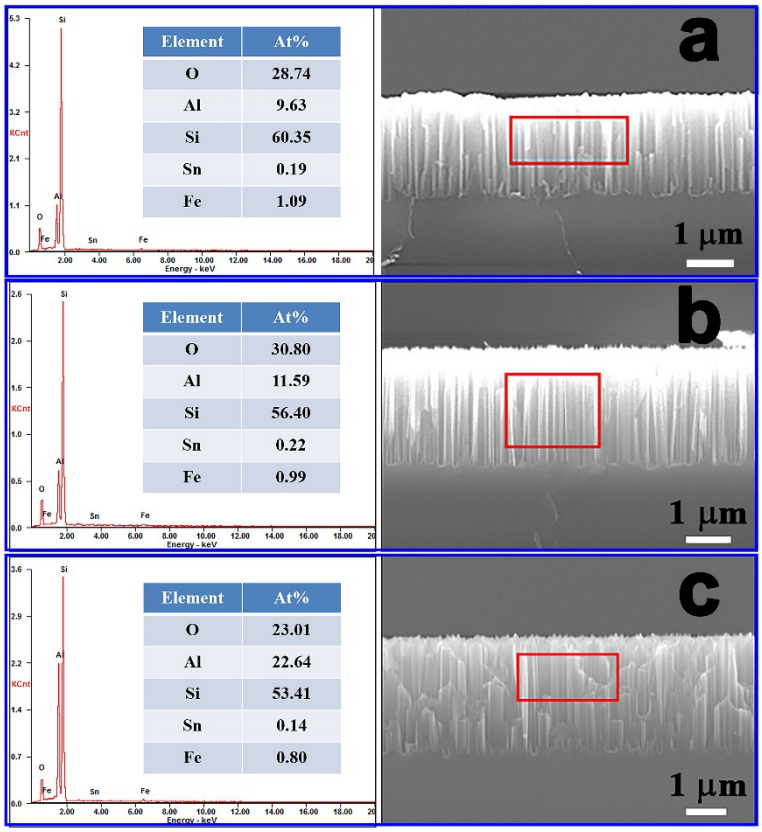

Fig. S9 EDS comparison and corresponding SEM images in the (a) SiNWs/Sn@α-Fe_2O_3, (b) SiNWs/Sn@α-Fe_2O_3/Al_2O_3 and (c) SiNWs/Al_2O_3/Sn@α-Fe_2O_3 photoanodes, respectively.

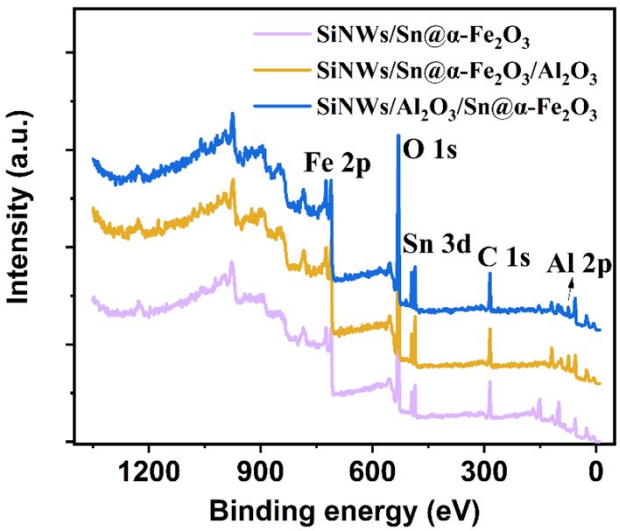

Fig. S10 XPS spectra of the SiNWs/Sn@α-Fe_2O_3, SiNWs/Sn@α-Fe_2O_3/Al_2O_3, SiNWs/Al_2O_3/Sn@α-Fe_2O_3 photoanodes, respectively.

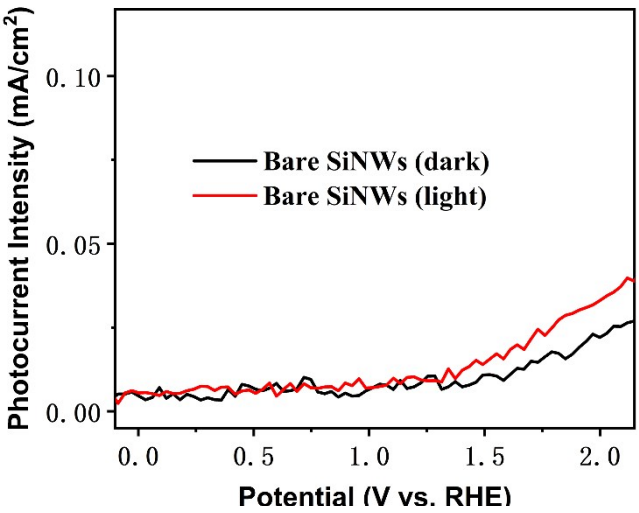

Fig. S11 Linear scan voltammograms of SiNWs in 1 M NaOH electrolyte in dark and under simulated AM 1.5G illumination.

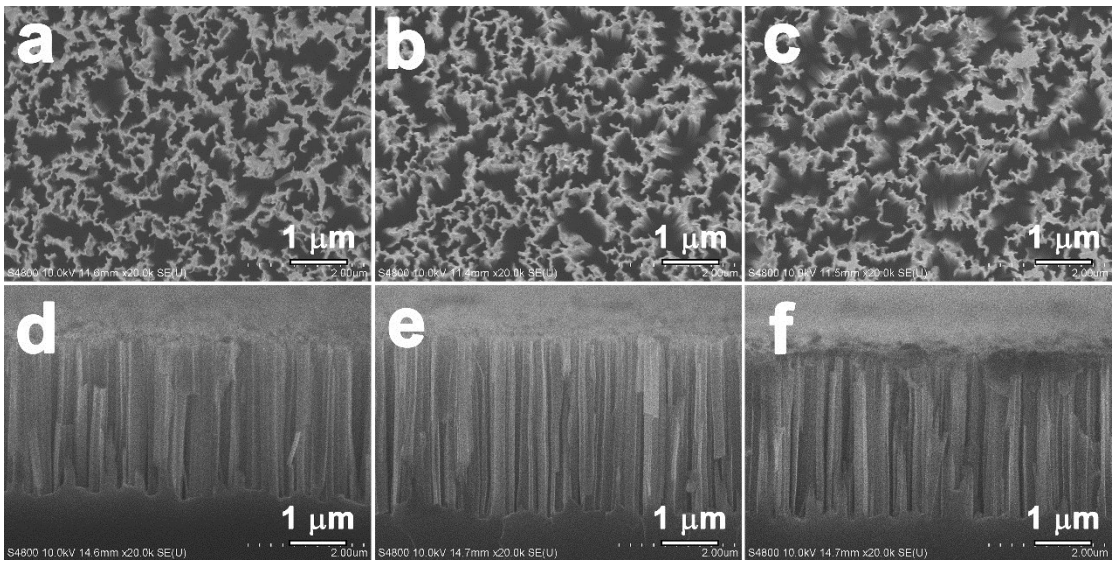

Fig. S12 SEM images of the SiNWs/Sn@α-Fe_2O_3 with different thicknesses of Sn@Fe_2O_3 film. (a–c) and (d–f) are top-view and cross-section SEM images, respectively. (a and d), (b and e) and (c and f) represent the Sn@α-Fe_2O_3 films prepared with 0.01 M, 0.02 M and 0.03 M $Fe(NO_3)_3$ precursor solutions, respectively.

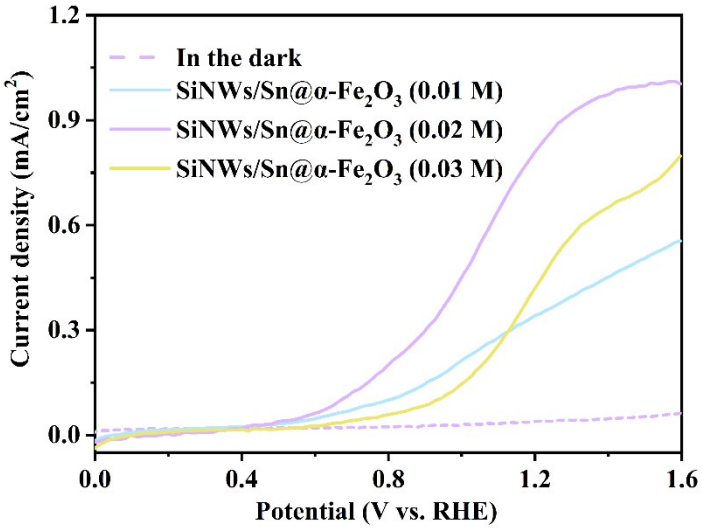

Fig. S13 *J-V* curves of the SiNWs/Sn@α-Fe_2O_3 prepared with 0.01 M, 0.02 M and 0.03 M $Fe(NO_3)_3$ precursor solutions.

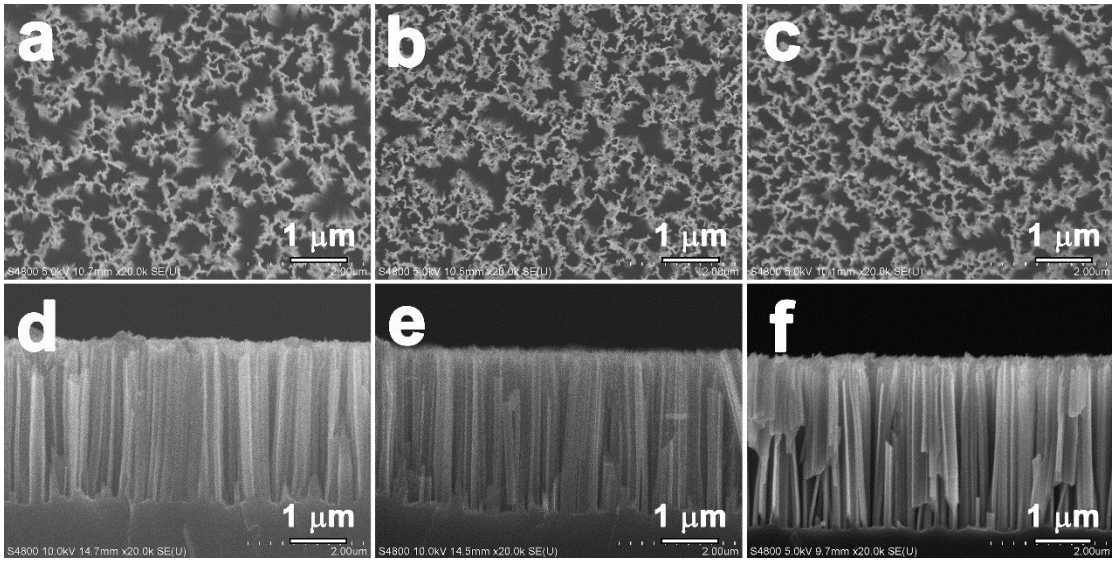

Fig. S14 SEM images of the SiNWs/Sn@α-Fe_2O_3/Al_2O_3 with different thicknesses of Al_2O_3 overlayer. (a–c) and (d–f) are the top-view and cross-section SEM images, respectively. (a and d), (b and e) and (c and f) represent the 5, 10 and 20 ALD-cycle Al_2O_3 coated on the SiNWs/Sn@α-Fe_2O_3, respectively.

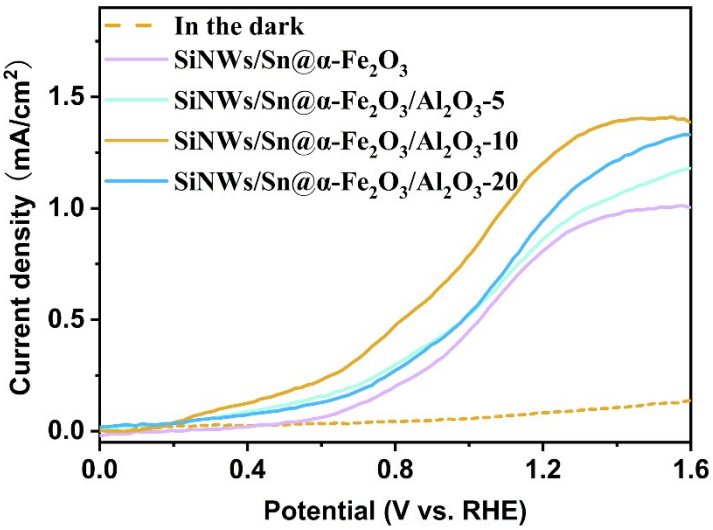

Fig. S15 *J-V* curves of the SiNWs/Sn@α-Fe_2O_3/Al_2O_3 photoanodes with 5, 10 and 20 ALD-cycle Al_2O_3.

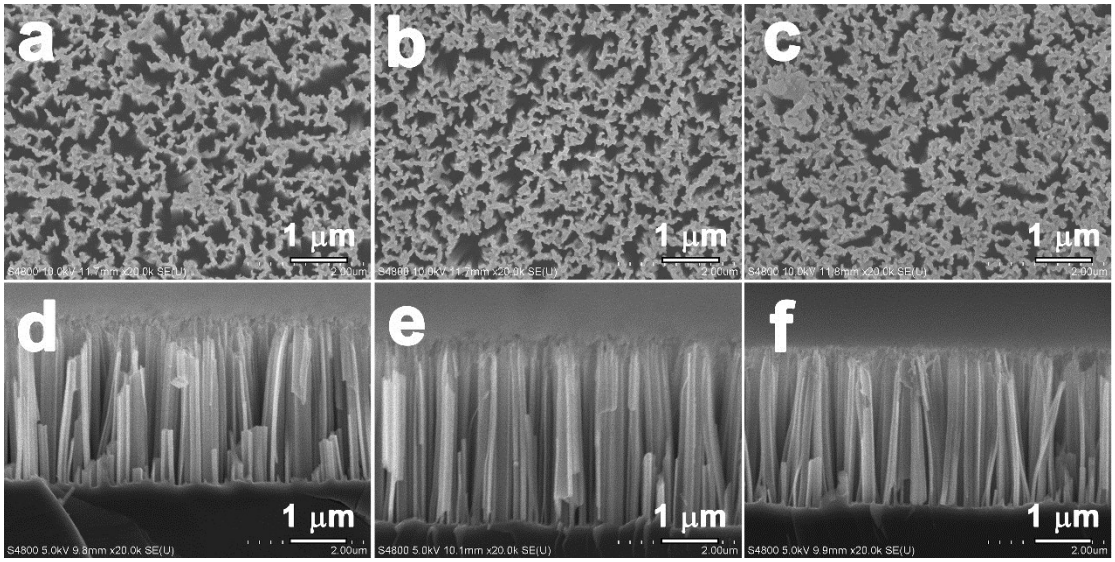

Fig. S16 SEM images of the SiNWs/Al_2O_3/Sn@α-Fe_2O_3 with different thicknesses of Al_2O_3 interlayer. (a–c) and (d–f) are the top-view and cross-section SEM images, respectively. (a and d), (b and e) and (c and f) represent the 70, 90 and 110 ALD-cycle Al_2O_3 coated on the SiNWs substrate and buried by the Sn@α-Fe_2O_3 film, respectively.

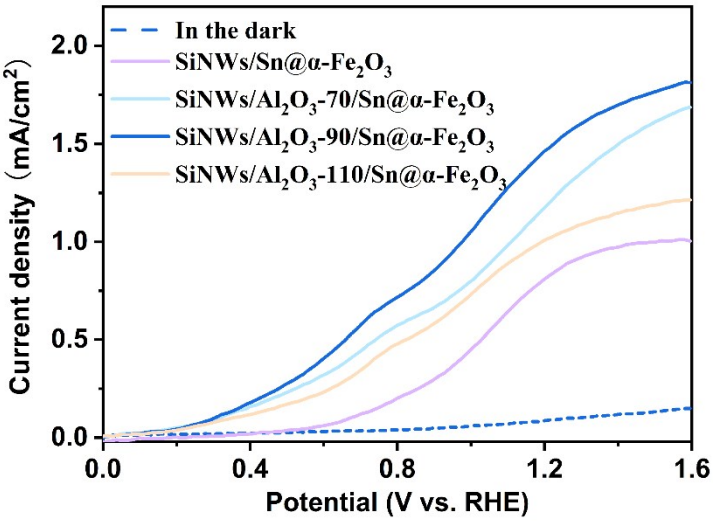

Fig. S17 *J-V* curves of the SiNWs/Al_2O_3/Sn@α-Fe_2O_3 photoanodes with 70, 90 and 110 ALD-cycle Al_2O_3.

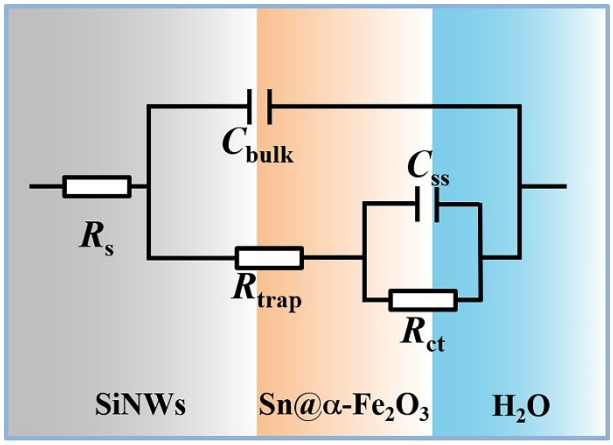

Fig. S18 The employed equivalent circuit for EIS analysis.

Table S1 The fitted values of the simulation parameters.

Sample	$R_S(\Omega)$	$R_{trap}(\Omega)$	C_{bulk}(F)	$R_{ct}(\Omega)$	C_{SS}(F)
SiNWs/Sn@α-Fe_2O_3	4.8	100.2	3.5×10^{-7}	4646.0	5.1×10^{-6}
SiNWs/Sn@α-Fe_2O_3/Al_2O_3	6.8	39.1	1.5×10^{-7}	4610.0	5.2×10^{-6}
SiNWs/Al_2O_3/Sn@α-Fe_2O_3	5.4	93.1	1.6×10^{-7}	1761.0	6.7×10^{-6}

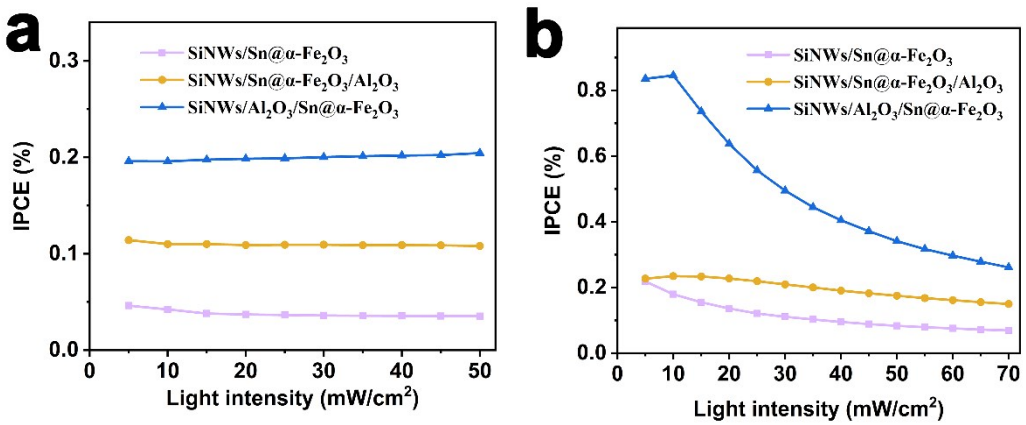

Fig. S19 Incident photon-to-current conversion efficiency (IPCE) as a function of light power density of the SiNWs/Sn@α-Fe_2O_3, SiNWs/Sn@α-Fe_2O_3/Al_2O_3, SiNWs/Al_2O_3/Sn@α-Fe_2O_3 photoanodes under (a) λ=365 nm and (b) λ=620 nm irradiation.